ARCHIVIO ISTITUZIONALE
DELLA RICERCA

Alma Mater Studiorum Università di Bologna
Archivio istituzionale della ricerca

Development and software in the loop validation of a Model-based water injection combustion controller for a GDI TC engine

This is the final peer-reviewed author's accepted manuscript (postprint) of the following publication:

Published Version:
Ranuzzi F., Cavina N., Brusa A., De Cesare M., Panciroli M. (2019). Development and software in the loop validation of a Model-based water injection combustion controller for a GDI TC engine. SAE International [10.4271/2019-01-1174].

Availability:
This version is available at: https://hdl.handle.net/11585/703895 since: 2024-05-10

Published:

DOI: http://doi.org/10.4271/2019-01-1174

Terms of use:

Some rights reserved. The terms and conditions for the reuse of this version of the manuscript are specified in the publishing policy. For all terms of use and more information see the publisher's website.

This item was downloaded from IRIS Università di Bologna (https://cris.unibo.it/).
When citing, please refer to the published version.

(Article begins on next page)

18 November 2026

2019-01-1174

Development and Software in the Loop Validation of a Model-based Water Injection Combustion Controller for a GDI TC Engine

Author, co-author (Do NOT enter this information. It will be pulled from participant tab in MyTechZone)

Affiliation (Do NOT enter this information. It will be pulled from participant tab in MyTechZone)

Abstract

Turbocharged (TC) engines work at high Indicated Mean Effective Pressure (IMEP), resulting in high in-cylinder pressures and temperatures, improving thermal efficiency, but at the same time increasing the possibility of abnormal combustion events like knock and pre-ignition. To mitigate knocking conditions, engine control systems typically apply spark retard and/or mixture enrichment, which decrease indicated work and increase specific fuel consumption.

Many recent studies have advocated Water Injection (WI) as an approach to replace or supplement existing knock mitigation techniques. Water reduces temperatures in the end gas zone due to its high latent heat of vaporization. Furthermore, water vapor acts as diluent in the combustion process.

In this paper, the development of a novel closed-loop, model-based WI controller is discussed and critically analyzed. The innovative contribution of this paper is to propose a control strategy based on an analytical combustion model that describes the relationship between the combustion phase and the Spark Advance (SA), considering also the effects of the injected water mass. Such model is calibrated with experimental data acquired during dedicated experimental tests on a GDI TC engine, equipped with a prototype Port Water Injection (PWI) system.

At first the WI setup is described, and the main experimental data are presented and processed for model identification. Two algorithm versions are then explained in detail and implemented in Simulink environment, with a Real-Time (RT) oriented approach. In the last part of this work, the WI control strategy is tested in a Software in the Loop (SiL) system, coupled with a one-dimensional Fast Running Engine Model (FRM). The controller is tested on several engine points in steady state and transient conditions and the Root Mean Squared Error (RMSE) is calculated for the control targets. In this way, the performance of the model-based controller is verified, and the two versions of the algorithm are quantitatively compared.

Introduction

Recently, the use of water in internal combustion engines to supplement the air-fuel mixture has rapidly gained relevance for modern boosted and downsized GDI SI engines [1,2,3,4]. At high load these engines are exposed to knock and even preignition or super-knock events, due to high in-cylinder pressure, and therefore engine combustion control is usually designed to retard the combustion phasing. This procedure, in addition to the need to enrich AFR value of the mixture at high power to reduce exhaust gas temperature, inevitably affects performance and efficiency. Thus, Water Injection is recognized to be one of the key technologies for enabling higher efficiency spark ignited gasoline engines [5,6,7]. Water Injection enables higher compression ratios up to 14 by mitigating heat release rates and knock tendency at high loads. Therefore, optimum spark advance can be maintained over a wider area of engine operating map, relaxing the knock limited spark advance (KLSA) constraint. Furthermore, WI allows reducing thermal stresses on the turbine and exhaust system components, without fuel enrichment. The addition of water produces air cooling due to evaporation and charge dilution (EGR-like), which slows down the combustion rate and reduces peak temperatures [1,2,8,9,10].

In [4] a Port Water Injection experimental setup is described, and an experimental campaign focused on WI effects on combustion is shown. The tests consist in SA sweeps performed for different values of the injected water mass, for each single operating point. The water mass injected in the runners is defined by the parameter r:

$$r = \frac{m_w}{m_f} \quad (1)$$

Where m_w and m_f are the masses of water and fuel introduced during a cycle, respectively. The data analysis shows two fundamental effects related to the increase of r: a gradual reduction of knock intensity close to Maximum Brake Torque (MBT) SA and a proportional delay of combustion phasing. Instead, the MBT value is slightly affected by r variations and there is a little offset of optimum 50% Mass Fraction Burned (MFB50) angle. These results suggest that it is possible to use WI to reduce knock intensity, allowing to achieve the combustion phase that ensures MBT even at high load, without exposing engine to damage. The achievement of this goal requires the identification of the proper combination of r and SA values to be applied at every operating condition. The value of r must be chosen as the smallest value able to guarantee the necessary mitigation of dangerous events to keep knock level under a defined threshold, while MFB50 is maintained at optimum angle. On the other hand, SA must be defined to achieve the optimum MFB50 angle, considering the delay induced by water addition. This paper describes the development of an analytical control-oriented combustion model to ensure the highest combustion efficiency at high load using WI, by the determination of optimal SA values for given operating conditions (engine speed, load and injected water mass). This approach allows implementing such relationship in a simple way, with an extremely low computational effort. In fact, the model is based on the parabolic trend of the MFB50 with respect to the SA, and this can be implemented with fast calculations, which are particularly important for real-time control strategies. On the other hand, the necessity of a 4-dimensional lookup table is avoided (the SA should be mapped on a grid of different values of engine speed,

load, injected water mass and MFB50). Moreover, the analytical approach captures the physical trend of the SA, which would be neglected by mapping some values in a lookup table. The main innovation of this work is to implement such analytical combustion model in a real-time control strategy, demonstrating its ability to maximize efficiency by accurately tracking target MFB50 angles also under knock-limited operation, while guaranteeing engine integrity and minimizing water consumption.

The authors innovative contribution is also highlighted by the poor presence of papers focused on semi-empirical and analytical models for controlling the combustion process using additional control actuators, such as water injectors. Most of the recent and interesting contributions in this field are in fact based on more complex modeling techniques and approaches, such as neural networks [11], or high-fidelity combustion models [12, 13].

The Water Injection based Combustion Controller (WICC) has been developed using a combined approach of experimental investigation and simulation environment:

- First, an experimental investigation has been carried out to investigate the effects of several values of *r* on combustion. Tests have been carried out over the most critical engine operating region in terms of knock tendency, applying SA sweeps for each *r* value.
- Then, experimental data have been processed (considering the mean cylinder) to define a WI Combustion Model (WICM) able to compute the optimal SA depending on MFB50 target and injected water mass. Three different models are presented and critically compared.
- In the third stage, the WICM has been implemented within the Open Loop (OL) branch of an innovative WI Combustion Controller (WICC), which has been tested via Software in the Loop (SiL), coupling the algorithm to a one-dimensional engine simulator. The WICC has been proposed first with a Closed Loop on Knock Index, and then with an additional MFB50 Closed Loop contribution.

The implementation of the two CL branches is motivated by the aim of exploring all the achievable benefits in presence of both Knock Index and MFB50 measurements. Both inputs have been obtained by processing in-cylinder pressure signals. The next step of the project consists in substituting in-cylinder pressure signals with other signals, available on-board, such as engine block vibrations or ionization current. In particular, the possibility of identifying the MFB50 by real-time processing the accelerometer signal has been demonstrated in a previous work, as reported in [14].

Experimental Campaign

Experimental Setup

Tests have been performed on a 4-cylinder GDI TC engine, equipped with a prototypal port water injection system. Further details are described in [4]. The main features of the experimental setup are shown in Table 1. In-cylinder pressure signals are sampled at 200 kHz and knock intensity is measured using Maximum Amplitude of Pressure Oscillations (MAPO) index, defined as:

$$MAPO = \max(|p_f|) \qquad (2)$$

Where p_f is the high-pass filtered in-cylinder pressure signal, with a 5 kHz cutoff frequency.

Table 1. GDI TC Engine features.

Engine displacement	1389.9 cc (4 cylinder)
Stroke	75.6 mm
Bore	76.5 mm
Connecting Rod	144.0 mm
Compression ratio	10:1

The experimental campaign has been designed to explore the effects of WI in a wide operating engine field, focusing on the areas with high knock tendency. Therefore, a grid of operating points has been defined by 2 levels of loads and 4 engine speeds, as shown in Table 2. The load is expressed with the Net Load (NL) parameter defined in Equation (3):

$$NL = pressure_{manifold} * \eta_{intake} \qquad (3)$$

Where η_{intake} is a factor that takes into account pressure drop within intake runners and valves.

Table 2. Experimental grid operating points.

Engine point	Speed [RPM]	NL [bar]	Lambda	r
1	1500	0.86	1	0:0.2:0.8
2	1500	1.00	1	0:0.2:0.8
3	2500	1.20	1	0:0.2:0.8
4	2500	1.40	1	0:0.2:0.8
5	3500	1.45	1	0:0.2:0.8
6	3500	1.8	1	0:0.2:0.8
7	4500	1.30	1	0:0.2:0.8
8	4500	1.50	1	0:0.2:0.8

For each operating point the same investigation methodology has been carried out. It consists in the execution of a specific SA sweep at different *r* values that are applied in ascending sequence from 0 to 0.8, with incremental steps of 0.2. The angular SA step used in every sweep depends on Knock Limited Spark Advance (KLSA), and near Knock Limit Spark Advance (nKLSA). Such indexes define the SA angle that causes a knock tendency close to the safety threshold (KLSA) and close to 60% of the same threshold (nKLSA). The knock intensity is quantified as the 98th percentile of MAPO. It is defined as the value below which 98 percent of MAPO index values are contained, in a sorted set of consecutive combustions. The threshold for this index is defined according to Equation (4):

$$MAPO98_{threshold} = \frac{RPM}{1500} \qquad (4)$$

The first element (*SAfirst*) of each SA sweep is defined by Equation (5), unless the limit on maximum exhaust gas temperature is exceeded:

$$SAfirst = SAbase + \frac{3*r}{0.2} \qquad (5)$$

In which:

- *SAbase* is the calibration value of SA
- The 3 CA offset has been arbitrarily assumed as the average value of combustion delay related to a step of 0.2 *r* [4]

In conclusion the SA sweeps are carried out with the following specifications:

1. Angular steps of 3CA from *SAfirst* to nKLSA
2. Angular steps of 1 CA from nKLSA to KLSA

This methodology has been conceived to obtain a wide vision of WI effects on MFB50 and, at the same time, to investigate with more accuracy all combustion indexes near the KLSA area.

WI Combustion Model

Experimental data has been processed, point by point, to analyze the relationship between SA and MFB50, for each tested *r* value. For a single spark sweep, the most appropriate fitting function to analytically describe the relationship between SA and MFB50 is the quadratic polynomial, as clearly shown in Figure 1. Such figure displays some spark sweeps for different values of parameter *r*, highlighting the influence of such parameter on the trend that could be identified in the absence of water injection.

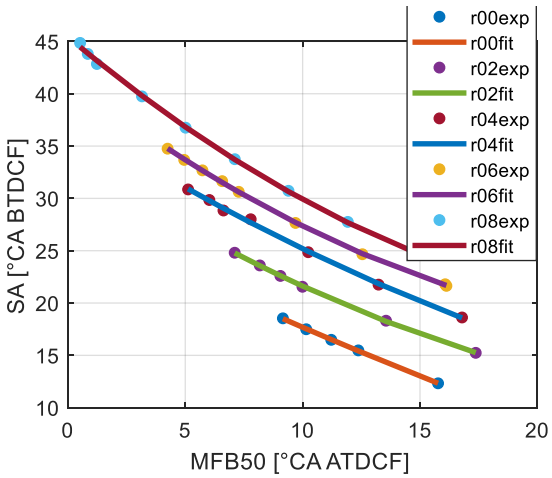

Figure 1. Parabolic fitting of the SA trend with respect to MFB50, for the engine point characterized by NL=1.2 and RPM=2500, and for different water-to-fuel mass ratios. It is an example of the parabolic trend that links the SA to the MFB50 for fixed operating conditions.

The Equation (6) defines the polynomial fitting of the SA on MFB50 domain.

$$SA = a\,MFB50^2 + b\,MFB50 + c \qquad (6)$$

This analysis allows to conceive a WI Combustion Model that processes the RPM, NL, *r* and the target of MFB50 as inputs, to compute the corresponding SA to be applied. The base concept is to calculate the parameters *a*, *b* and *c* of the parabolic function and investigate the analytical dependence of each parameter from the *r* value. Three different methods have been designed to build such model, and the respective performances have been evaluated by comparing experimental and modeled SA. The fitting quality has been quantified for each proposed method by evaluating the correlation coefficient.

Polynomial Method

Through the parabolic fitting of MFB50 and SA data for each engine point and for each value of *r*, the three coefficients *a*, *b*, *c*, (called Parabolic Coefficients), have been identified. Each parameter has been fitted with a polynomial function of RPM and NL (Net Load), for each value of *r*. The resulting equation for *a*, *b* and *c* is the following:

$$PCoeff = p_{00} + RPM * p_{10} + NL * p_{01} + \ldots$$

$$+ RPM * NL * p_{11} + RPM^2 * p_{20} \qquad (7)$$

Where p_{00}, p_{10}, p_{01}, p_{11}, p_{20}, are called Surface Coefficients. In Figure 2 are shown all the resulting surfaces, for r = 0.

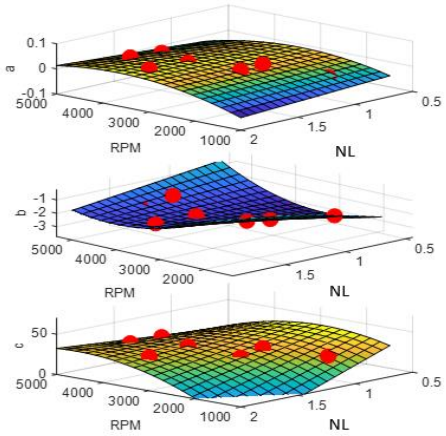

Figure 2. Fitting surfaces of the parabolic coefficients in (RPM, NL) domain, for *r*=0.

Every single surface is described by a set of 5 Surface Coefficients p_{xx} and each coefficient features a quite constant slope in *r* domain as displayed in Figure 3, so it can be fitted with a linear function, as shown in Eq. (8).

$$p_{xx} = o_{xx} + r * g_{xx} \qquad (8)$$

Where o_{xx} is the constant term and g_{xx} the curve slope.

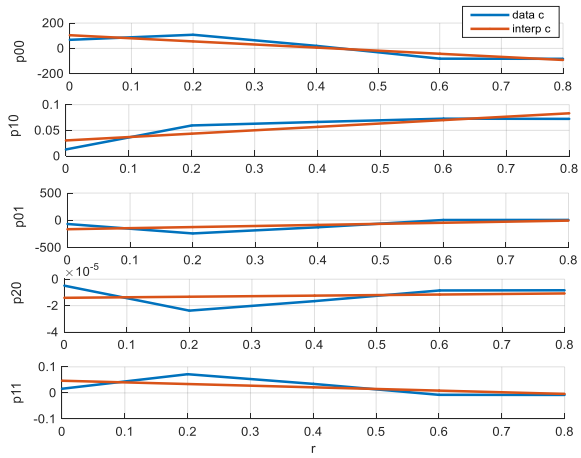

Figure 3. Fitting of surface coefficients by linear function, for parameter c.

Figure 4 shows a block diagram of the model based on polynomial fitting, relating the SA to the MFB50 target, for different combinations of *r*, RPM, and NL (i.e., the model inputs).

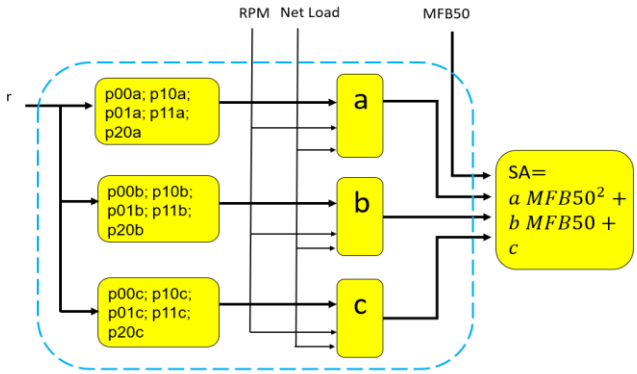

Figure 4. Combustion Model with Polynomial Method.

Effects Separation Method 1-D

To verify the possibility of reducing the computational load and the allocated memory, other two implementation methods of the MFB50-SA open-loop combustion model have been investigated. The first one is the simplest and fastest one, where the effects of water-to-fuel ratio, described by the parameter *r*, are considered to be independent of speed and load. With this method, the mean surface for *r*=0.5 of parameters *a*, *b* and *c* has been calculated and it has been defined as the reference between all surfaces obtained for the different *r* values (Figure 5). Every coefficient has then been identified for all values of parameter *r*, for each engine point. Such values have been normalized with respect to the value which corresponds to *r*=0.5. The final trend is then described by the mean of the normalized values. In this way, such curve represents the gain of the related parameter which adapts the reference parameter value when *r* is different from 0.5. The three normalized curves are discretized as arrays called *Ka*, *Kb*, *Kc*, with *r* as input. In Figure 6 the trend of *Ka* for each engine point and the mean curve are shown.

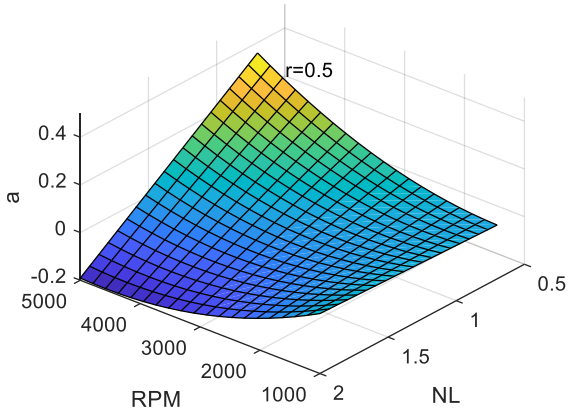

Figure 5. The calculated surface of parameter *a*, for *r*=0.5.

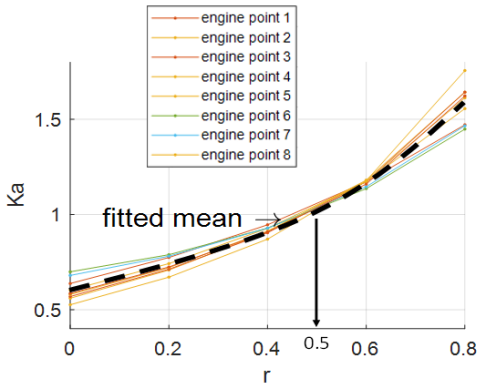

Figure 6. Normalized curve *Ka*.

In other words, the final approximated coefficient value can be recovered by multiplying the gain identified by the injected water mass *r* with the respective value of the same parameter at *r*=0.5, which depends on the engine point (RPM, NL). Figure 7 shows a block diagram of the model based on full mono-dimensional effects separation.

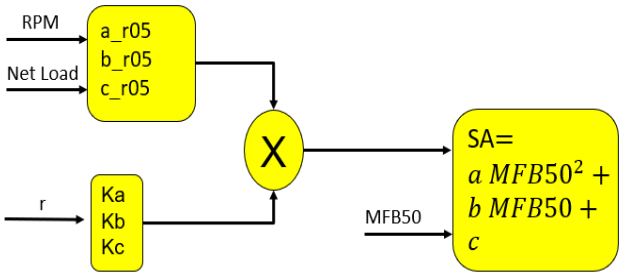

Figure 7. Combustion model with Separation Effect 1-D.

Effects Separation Method 2-D

In this case, a degree of complexity is added to the previous model, by mapping the "correction" factors *Ka*, *Kb* and *Kc* as two-dimensional functions, depending on *r* and on another influent parameter, chosen between NL and RPM. To identify the most influencing factor, every coefficient has been displayed trough two different representations, for each engine point. First, as surfaces on *r*-RPM domain, and second, as surfaces on *r*-NL domain. For both representations, a normalization over the 0.5 *r* value has been

investigated, and the mean of all normalized surfaces has been computed and displayed. The comparison between the two representations highlights that NL has more influence on surface gradient than RPM (Figure 8). Thus, in this method the gain has been replaced by a 2-D matrix with NL and *r* as inputs. Figure 9 shows a block diagram of the model based on partial effects separation.

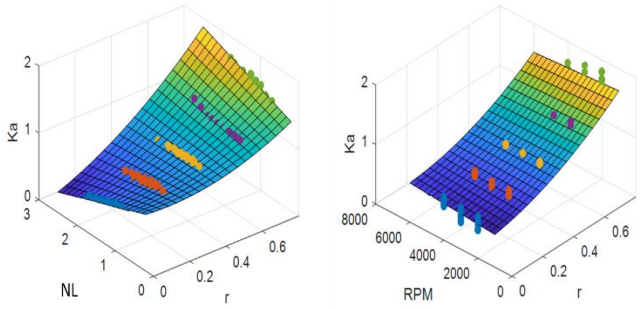

Figure 8. Average surface *Ka* on NL-*r* domain (left) and on RPM-*r* domain (right).

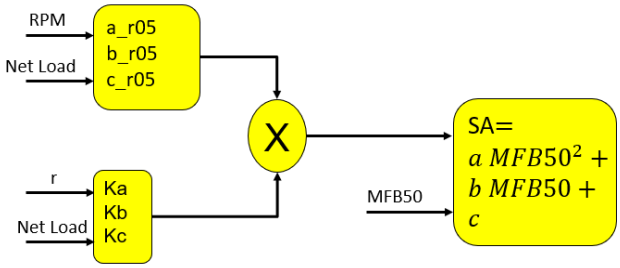

Figure 9. Combustion model with Separation Effect 2-D.

Comparison by Correlation Coefficient

To evaluate the accuracy of each method, the relative Correlation Coefficients ρ have been computed, as defined by Equation 9:

$$\rho(A,B) = \frac{1}{N-1} * \sum_{i=1}^{N} \left(\frac{A_i-\mu_A}{\sigma_A}\right) * \left(\frac{B_i-\mu_B}{\sigma_B}\right) \qquad (9)$$

Where:

- A is the array of the computed SA values by the different methods
- B is the array of experimental SA values
- μ_A and σ_A are the mean and standard deviation of A
- μ_B and σ_B are the mean and standard deviation of B

As shown in Table 3, the polynomial method produces the highest ρ value. Thus, this approach has been selected for control implementation. Also because in this phase of the project the computational burden of the controller has not been considered as a hard constraint.

Table 3. Correlation Coefficient values for the three different methods used to define the combustion model. The green boxes highlight the best result and the corresponding method.

Method	Polynomial	Eff. Sep. 2-D	Eff. Sep. 1-D
ρ	0.99	0.97	0.91

WI-based Combustion Control

The definition of a combustion model able to compute the SA required to reach the MFB50 target at a specific *r*, allows designing a WI combustion controller oriented to knock mitigation at high loads, while keeping MFB50 at its optimum value. The WI-based Combustion Controller (WICC) has been designed with both Open Loop (OL) and Closed Loop (CL) branches. The OL requires as inputs the water-to-fuel mass ratio (*r*) and the MFB50 target. For this reason, two look-up tables (one for *r* and one for MFB50) have been defined. The CL operates to maintain the measured MAPO98 close to the threshold, with a statistical approach (MAPO98 is the 98th percentile of the MAPO distribution considered in the given buffer of MAPO values). A second version of the CL controller has also been developed. Such algorithm is able to control also the MFB50 by closing the loop on its measurement, to overcome errors of the combustion model and to meet the target. The performance of the two algorithms are evaluated simulating several steady state engine points and several transient conditions. The results quality is then highlighted with the Root Mean Squared Error (RMSE) between the mean MFB50 and the corresponding target. The same parameter has been used for the MAPO98.

CL on MAPO98

The developed OL branch requires a MFB50 target map and a *r* map, both based on RPM and NL (Net Load), to provide the necessary inputs for the combustion model. The first one provides the MFB50 target angle, and the second a *r* value, calibrated with the same methodology for all the investigated experimental points. The methodology consists of three steps. At first, the required SA angles to target the optimum MFB50 (arbitrarily fixed to 8°CA ATDCF) are computed by processing the related parabolic function, described by Eq.(10), for all injected water masses, for each experimental point (Figure 10):

$$SA_{opt} = a\ MFB50_{opt}{}^2 + b\ MFB50_{opt} + c \qquad (10)$$

Where:

- *a*, *b* and *c* are the coefficients of the parabolic function *SA=f(CA)*, for a *r* value and for a fixed engine point
- SA_{opt} is the spark angle which guarantees the $MFB50_{opt}$

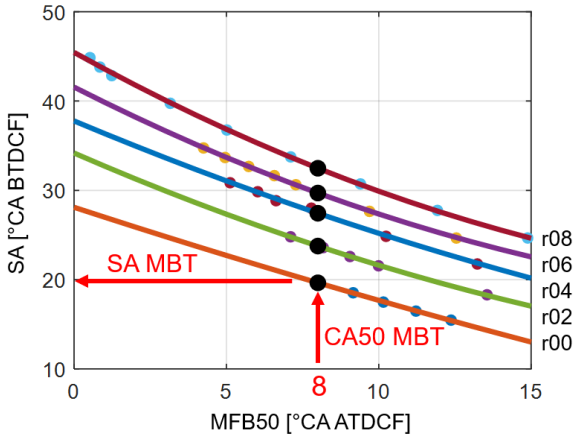

Figure 10. SA Maximum Brake Torque (MBT) determination procedure.

Then the MAPO98 values corresponding to optimum SA are determined by evaluating the exponential function described by Eq.(11), one for each *r* value (colored curves in Figure 11):

$$MAPO98_{opt} = g\ SA_{opt}{}^{f} + k \qquad (11)$$

Where:

- *g*, *f* and *k* are the parameters of the exponential function *MAPO98=f(SA)*, for a *r* value and for a fixed engine point
- $MAPO98_{opt}$ is the MAPO98 value obtained for the $MFB50_{opt}$

At last, optimal MAPO98 values are fitted with another parabolic function, described by Eq.(12), on *r* domain (red curve in Figure 11), and through intersection with MAPO98 threshold (KL, in Figure 11), it is possible to evaluate the minimum *r* value that guarantees a permissible MAPO98 (equal to 0.2 in the example shown in Figure 11, where the corresponding SA MBT is also highlighted):

$$r_{map} = m\ MAPO98_{thr}{}^{2} + n\ MAPO98_{thr} + l \qquad (12)$$

Where:

- *m*, *n* and *l* are the parameters of the parabolic function $r=f(MAPO98_{opt})$, for each engine point
- r_{map} is the minimum *r* value which allows respecting the $MAPO98_{thr}$

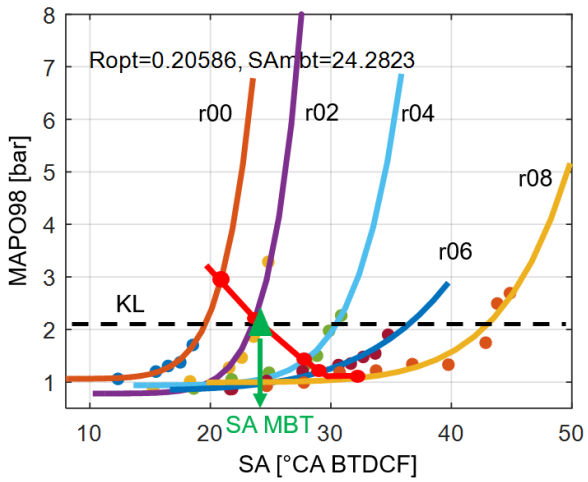

Figure 11. R map determination and related SA MBT.

When this value saturates at maximum *r* value allowed (arbitrarily fixed at 0.8), a spark retard is necessary to guarantee knock reduction. Thus, a new SA angle must be defined in the intersection between the exponential MAPO98 function calculated for *r*=0.8 and knock threshold (Figure 12, where SA ACT does not correspond to SA MBT):

$$SA_{act} = e^{\frac{\log\frac{MAPO98_{thr} - k_{08}}{g_{08}}}{f_{08}}} \qquad (13)$$

Where:

- g_{08}, f_{08} and k_{08} are the parameters of the exponential function *MAPO98=f(SA)* for *r*=0.8, for a specific engine point
- SA_{act} is the spark advance actuated to obtain a MAPO98 equal to the threshold

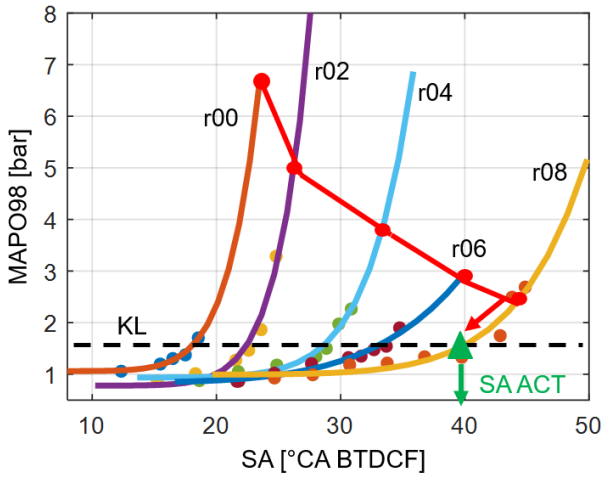

Figure 12. SA determination, when *r* is saturated to 0.8.

As a result, the MFB50 map provides the optimum value (equal to 8CA ATDCF) when $r < 0.8$ and a delayed value when $r = 0.8$. The experimental data demonstrate that this circumstance is never verified, and the parameter *r* does not saturate to the maximum value. Consequently, the MFB50 target is equal to 8 on the entire operating field. Moreover, the experimental tests have been carried out at the highest load for the tested engine speeds. Thus, for the operating filed characterized by lower load levels, the choice of a MFB50 target equal to 8 is absolutely legitimate. The resulting *r* map for the mean cylinder is shown in Figure 13. The consequent MFB50 target map within the explored range and for lower loads becomes a constant equal to 8. Outside the operative field explored during the experimental campaign, the maps trends have been linearly extrapolated.

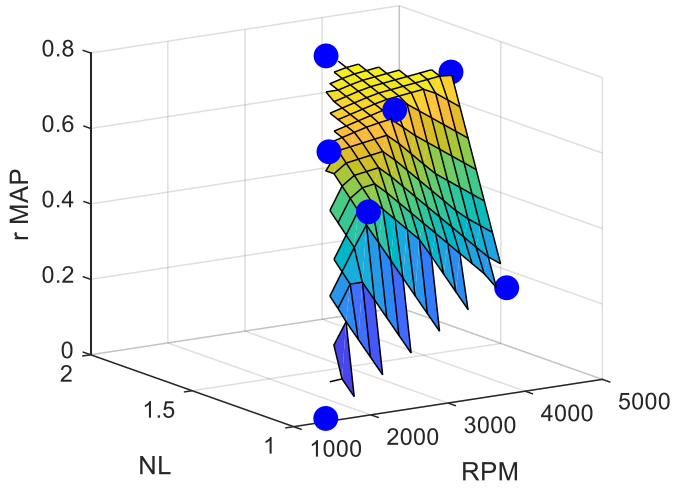

Figure 13. R map for the explored operative field.

The controller is also composed by a CL contribution (Figure 14). The first version of such closed-loop controller manages the

MAPO98, computed from MAPO measured cycle by cycle with in-cylinder pressure signal, by applying corrections to *r* and SA outputs. Basically, the implemented algorithm is based on a Proportional and Integral (PI) control system, which has been evolved to freely split the entire correction between the two levers on which the controller can act. The error between the measured MAPO98 and the corresponding threshold is translated into a proportional and integral correction through a gain scheduling PI structure. The resulting sum of two contributions is then converted in a percentage value which represents the total amount of the correction (Total Percentage Correction, TPC) which is required by the system for that specific operating condition. Such correction is then converted into *r* and SA variations, with a pre-defined logic. In this way, the TPC allows also to define a common reference to manage the two available actuators to control knocking events. When a *r* correction is applied, the OL chain compensates the final *r* value with the SA calculated by the Combustion Model, since the *r* correction is considered as input to such model (Figure 14). If the water-to-fuel ratio (*r*) reaches its saturation value (arbitrarily defined), to further reduce knocking a SA correction is also applied by the CL controller. The controller management of *r* and SA correction depends only on calibrations. Moreover, a protection strategy reacts proportionally to single MAPO events on the value of the TPC. Complete controller scheme is shown in Figure 14.

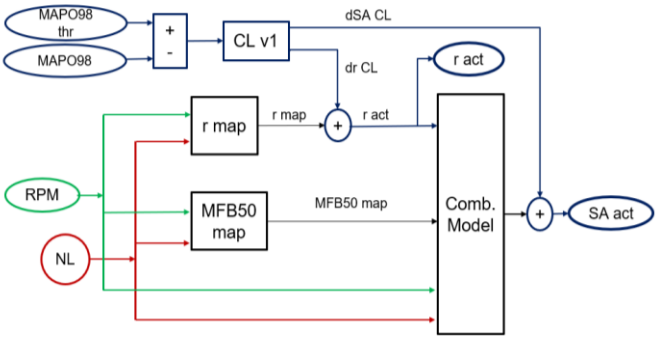

Figure 14. First version WICC layout.

CL on MAPO98 and MFB50

The CL chain has been further developed and it has been integrated with an algorithm which evaluates the SA corrections needed to respect the MFB50 target. In other words, the second version of the Closed Loop branch can calculate the SA variations also to reduce the error between the measured MFB50 (obtained from in-cylinder pressure signal) and the target one, which is the output of the map implemented within the OL chain. The MFB50 values are filtered with a moving average, to avoid the signal oscillations caused by the Cycle-to Cycle Variation (CCV) and to prevent a consequent unstable controller behavior. The idea is to create a second TPC related to MFB50 error (MFB50TPC), which defines the SA correction only when the engine works in not-knocking or light-knocking conditions. In particular, the MFB50TPC cannot be increased when the TPC related to the MAPO98 error is over the level which activates SA correction for knock mitigation. With such approach the final SA correction is always a sum of two contributions, and the definition of the actuation priority between the two CL controllers is not required. The new CL scheme allows to manage the SA variations, avoiding the overlap between opposite contributions which derive from the two different Total Percentage Corrections. When the TPC is increasingly close to the value which is fixed as the threshold which discriminates between acceptable and not-acceptable knock level, the maximum MFB50TPC is progressively reduced. So, with an appropriate calibration of the vector which defines the SA correction with respect to MFB50TPC, it is then possible to have two controllers that act corrections on spark advance (the first based on MAPO98 error and the second on MFB50 error) without conflicts. The complete layout of the second version of the Water Injection based Combustion Control is shown in Figure 15.

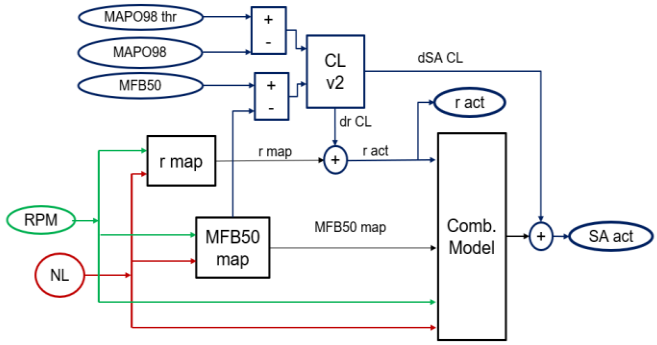

Figure 15. Second version WICC layout.

Software in the Loop Control Validation

The two versions of the WICC have been tested and validated via Software in the Loop (SiL) simulations. The controller has been coupled with a mono-dimensional mean-cylinder engine simulator which includes the WI, the CCV and a knock model. Such simulator consists in a GT Power model of the experimental setup, in which the combustion model has been calibrated via Three Pressure Analysis (TPA). The GT model has been also converted in a Fast Running Model (FRM), to test the controller in Real-Time (RT). Nine different engine points have been simulated, covering almost the entire boosted operating field. Of course, the lowest loads points have been neglected, because of the absence of knocking events and the consequent controller inactivity. The quality of the simulations results is defined through the R-squared index. Moreover, the simulations with the first version of the controller (that with the CL only on the MFB50 target), are also a validation of the reliability of the Combustion Model, because the accuracy on the MFB50 target is ensured only by the OL chain.

The Fast Running Model

In order to debug the controller algorithm, the WICC has been coupled with a GT Power model of the mean cylinder of the 4-cylinders of the GDI TC engine used during the experimental campaign. The predictive combustion model has been previously calibrated via Three Pressure Analysis, considering CCV and water injection effects, and the implemented knock model has been completely described, calibrated and validated in [12]. In this work, the GT model has been converted in an FRM. Such procedure consists in the reduction of engine model complexity, mainly through the combination of single ducts in parts with larger volumes. On the contrary, the combustion model and the intake and exhaust valves and ports are not modified, and this allows to maintain the predictive capabilities of the detailed model. While the accuracy of some ducts signals (like pressure and flow rate waves) is partially lost, the entire conversion process can be driven by the tolerance (imposed by the user) that has to be maintained for some combustion indexes (like maximum in-cylinder pressure, MFB50, etc.). In this way, the detailed model can be easily adapted for RT simulations [15]. Also,

the WI modelling has been modified to be in accordance with the new ducts configuration. As accurately described in a previous work [16], the WI system has been modelled with two injectors, where the first is a Port Water Injector (PWI) and the second is a Direct Water Injector (DWI). Through the calibration of parameters which define how the injected water mass is split between such injectors, the water vapor quantity and the angular duration of in-cylinder water evaporation can be correctly reproduced. Due to the new engine model layout, the WI previous configuration has been replaced with a single DWI layout and the parameters values have been replaced with a new calibration set. Figure 16 shows the layout of the FRM.

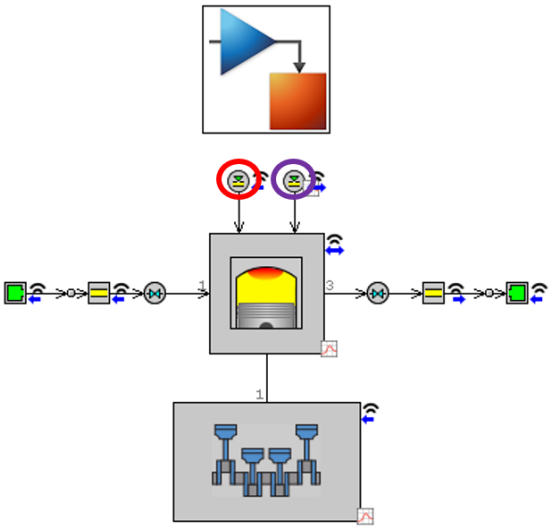

Figure 16. FRM layout. The red circle highlights the Direct Water Injector, the violet one highlights the fuel one.

Simulation Results

The FRM has been appropriately compiled and it has been consequently implemented in a 0-D co-simulation environment. The first simulations allow to identify the best calibration parameters set for the CL controller. They have been carried out for different engine points, in steady state and in transient conditions. During such simulations the PI controller applies *r* corrections which are then added to the map value, and CL contribution is not saturated above a specific value. This means the final *r* can assume too high values. Of course, this is not representative of a real application, in which the maximum *r* is certainly much lower, but such strategy allows studying the PI behavior on *r* and SA corrections also for high load conditions. It is important to accurately calibrate the CL parameters on the entire operating field.

In Figures 17, 18, 19 and 20 the results of simulations with the first version of the Water Injection based Combustion Control (characterized by the CL on MAPO98) are collected, for four different engine points. In Figure 17, 18 and 19 it has been simulated a medium NL condition and the CL works only with *r* corrections. In Figure 20 a high load engine point has been simulated and during the firsts 50 cycles it is possible to highlight the protection action with a SA decrement, due to a high MAPO cycle. For small errors on MAPO98 the PI manages the water mass and for high errors introduces also SA variations. The *r* corrections can have also a negative sign, to reduce the mapped water mass when the recorded MAPO98 is lower than the threshold (Figure 17). The CL parameters set has been chosen to guarantee a good correction stability and, at the same time, fast responses during transients. Figure 21 shows a transient simulation and during the rising ramp the CL is able to manage the knock intensity only with *r* corrections. In figures 17 through 21 the error between the mean MFB50 and the map value (the target) is due to inaccuracies of the Water Injection based Combustion Model used in the open-loop controller, which are quantified with the Root Mean Squared Error. The Table 4 collects the RMSE committed by the controller on the MFB50 and MAPO98 targets for each simulation, because they represent the indexes which allow to quantify the controller robustness. The errors are evaluated excluding the firsts cycles, due to the MAPO98 and MFB50 buffers which are filling and do not produce coherent values.

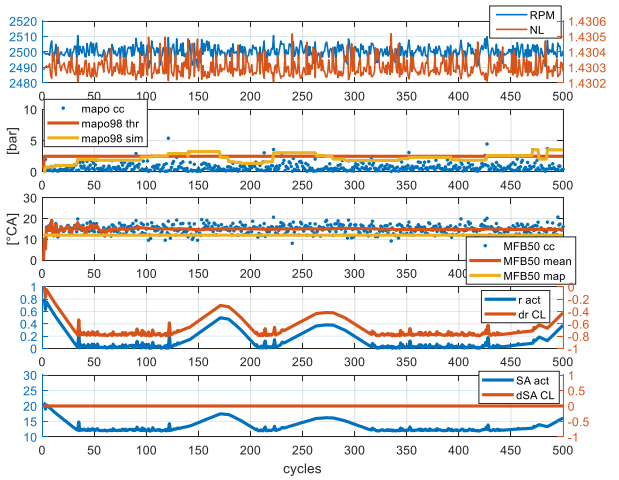

Figure 17. Steady state simulation results for engine point 2500 RPM, NL 1.43. Five subplots show (from top to bottom): RPM-NL, cycle-to-cycle recorded MAPO, MAPO98 and the MAPO98 threshold, cycle-to-cycle recorded MFB50, mean MFB50 and the corresponding target, the actuated *r* and the *r* correction calculated by CL chain, the actuated SA and the SA correction calculated by the CL chain.

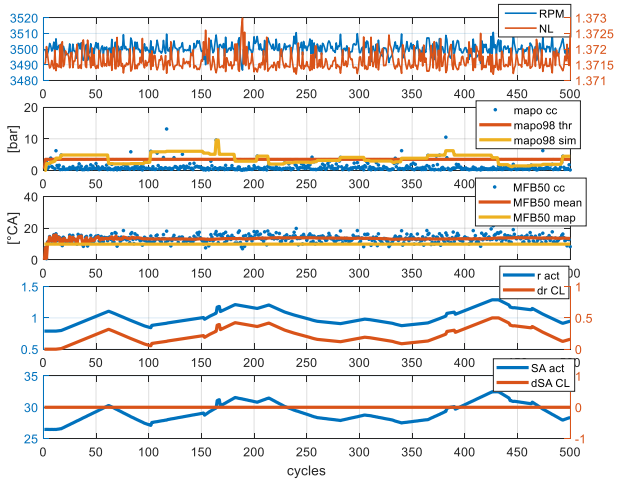

Figure 18. Steady state simulation results for engine point 3500 RPM, NL 1.37. Five subplots show (from top to bottom): RPM-NL cycle-to-cycle recorded MAPO, MAPO98 and the MAPO98 threshold, cycle-to-cycle recorded MFB50, mean MFB50 and the corresponding target, the actuated *r* and the *r* correction calculated by CL chain, the actuated SA and the SA correction calculated by the CL chain.

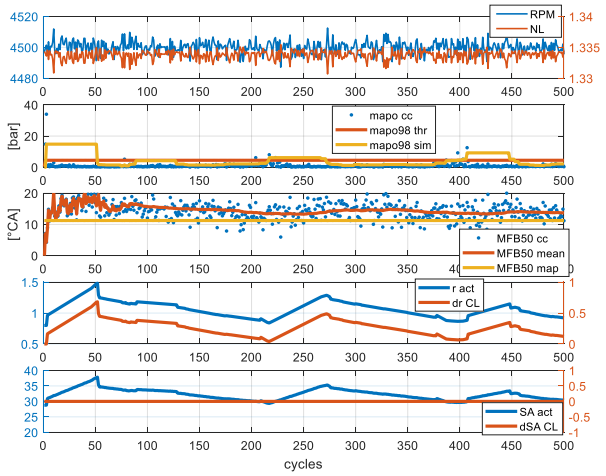

Figure 19. Steady state simulation results for engine point 4500 RPM, NL 1.33. Five subplots show (from top to bottom): RPM-NL, cycle-to-cycle recorded MAPO, MAPO98 and the MAPO98 threshold, cycle-to-cycle recorded MFB50, mean MFB50and the corresponding target, the actuated *r* and the *r* correction calculated by CL chain, the actuated SA and the SA correction calculated by the CL chain.

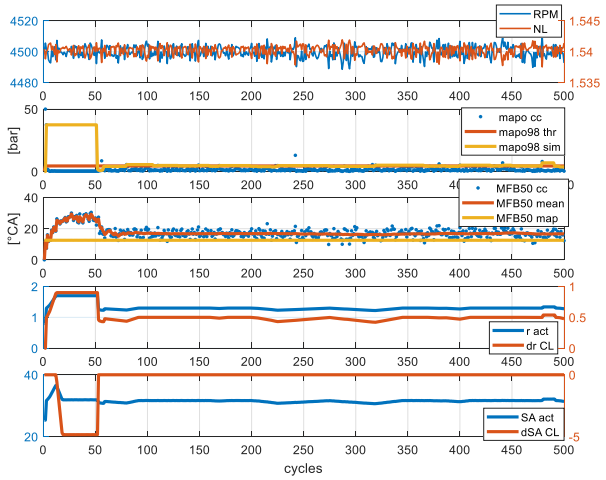

Figure 20. Steady state simulation results for engine point 4500 RPM, NL 1.54. Five subplots show (from top to bottom): RPM-NL cycle-to-cycle recorded MAPO, MAPO98 and the MAPO98 threshold, cycle-to-cycle recorded MFB50, mean MFB50 and the corresponding target, the actuated *r* and the *r* correction calculated by CL chain, the actuated SA and the SA correction calculated by the CL chain.

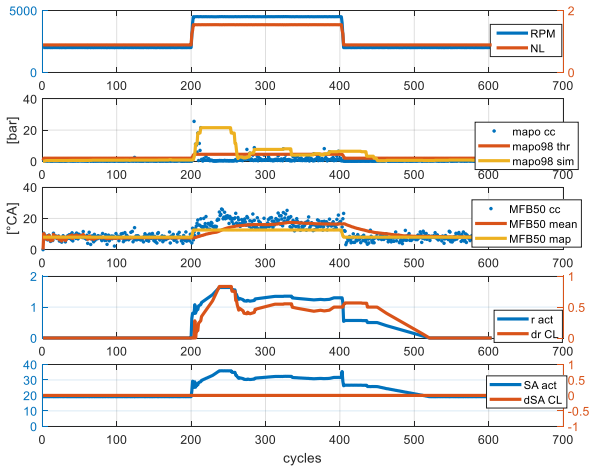

Figure 21. Transient simulation results. Five subplots show (from top to bottom): RPM-NL, cycle-to-cycle recorded MAPO, MAPO98 and the MAPO98 threshold, cycle-to-cycle recorded MFB50, mean MFB50and the corresponding target, the actuated *r* and the *r* correction calculated by CL chain, the actuated SA and the SA correction calculated by the CL chain.

Table 4. Root Mean Squared Errors for the validation simulations with the first version of the WI based Combustion Control. The mean value of the RMSE on mean (by moving average) MFB50 represents the accuracy of the Combustion Model.

Engine Point	RMSE MFB50 [°CA]	RMSE MAPO98 [bar]
RPM 2500 NL 1.43	1.81	0.55
RPM 3500 NL 1.37	2.55	1.24
RPM 4500 NL 1.33	2.10	0.63
RPM 4500 NL 1.54	1.61	0.81
RPM 2000-4500-2000 NL 0.8-1.7-0.8	1.75	4.02
Mean	1.96	1.45

Results of simulations with the second version of WICC (characterized by CL on MAPO98 and MFB50 target) are shown in Figures 22, 23, 24, 25 and 26. The CL on MAPO98 parameters values does not change, but during these simulations the final SA correction is the sum of two contributions (from MAPO98 and MFB50 CL controllers). The positive SA corrections are accepted only when the TPC is under a predetermined value. In Figure 24 it is possible to highlight negative and quick SA corrections in correspondence with a cycle characterized by a high MAPO level. In fact, in such simulation, the high MAPO value produces a high lower saturation of TPC, which is translated in an upper saturation of MFB50TPC to manage measured knock levels. This system avoids also on-off CL responses. In both figures it can be clearly seen that the MFB50 target is reached by the control system, thanks to the closed loop corrections evaluated by the MFB50 CL controller. The Figure 26 shows the transient simulation result during which the controller is able to maintain the mean MFB50 on the corresponding target. The CL calibration parameters have been set on values which guarantees fast responses of the controller to have quite fast

responses also in few simulated cycles, at the expense of the best stability. The Table 5 collects the RMSE for all simulations. The values highlight the reduction of the error on the MFB50 target.

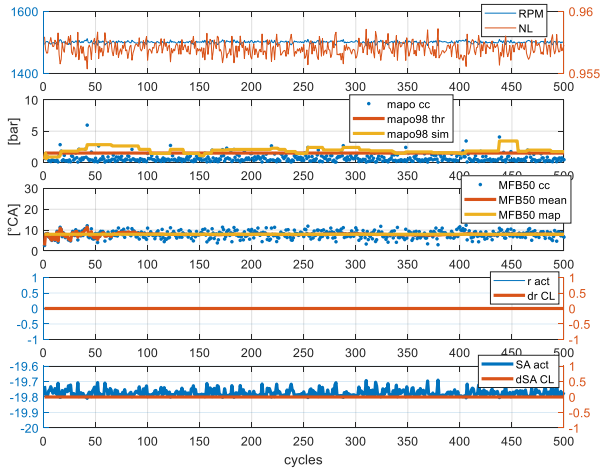

Figure 22. Steady state simulation results for engine point 1500 RPM, NL 0.95 with the CL on MFB50. Five subplots show (from top to bottom): cycle-to-cycle recorded MAPO, MAPO98 and the MAPO98 threshold, cycle-to-cycle recorded MFB50, mean MFB50 and the corresponding target, the actuated *r* and the *r* correction calculated by CL chain, the actuated SA and the SA correction calculated by the CL chain.

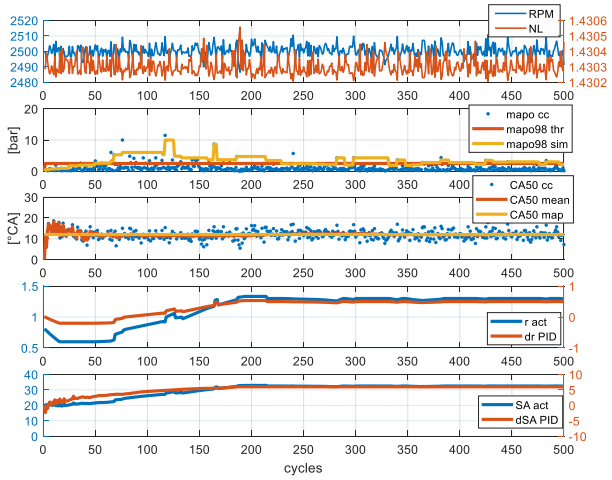

Figure 23. Steady state simulation results for engine point 2500 RPM, NL 1.43 with the CL on MFB50. Five subplots show (from top to bottom): cycle-to-cycle recorded MAPO, MAPO98 and the MAPO98 threshold, cycle-to-cycle recorded MFB50, mean MFB50and the corresponding target, the actuated *r* and the *r* correction calculated by CL chain, the actuated SA and the SA correction calculated by the CL chain.

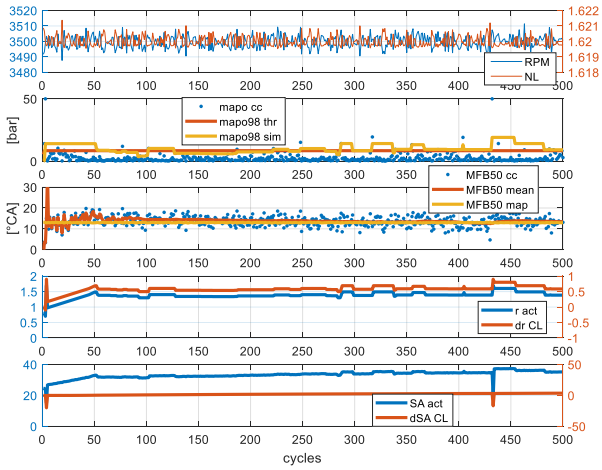

Figure 24. Steady state simulation results for engine point 3500 RPM, NL 1.62 with the CL on MFB50. Five subplots show (from top to bottom): RPM-NL, cycle-to-cycle recorded MAPO, MAPO98 and the MAPO98 threshold, cycle-to-cycle recorded MFB50, mean MFB50and the corresponding target, the actuated *r* and the *r* correction calculated by CL chain, the actuated SA and the SA correction calculated by the CL chain.

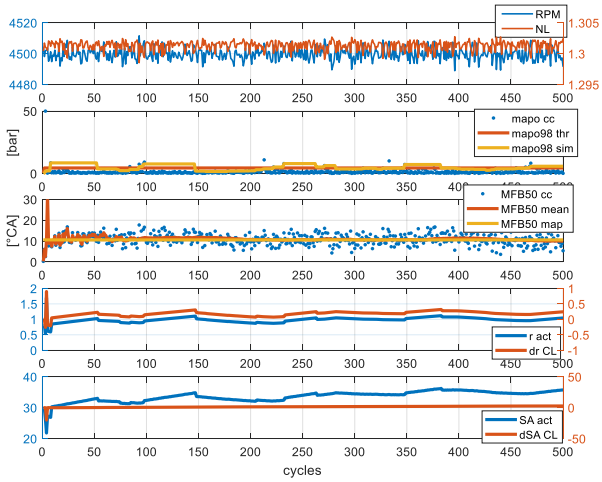

Figure 25. Steady state simulation results for engine point 4500 RPM, NL 1.3 with the CL on MFB50. Five subplots show (from top to bottom): RPM-NL cycle-to-cycle recorded MAPO, MAPO98 and the MAPO98 threshold, cycle-to-cycle recorded MFB50, mean MFB50 and the corresponding target, the actuated *r* and the *r* correction calculated by CL chain, the actuated SA and the SA correction calculated by the CL chain.

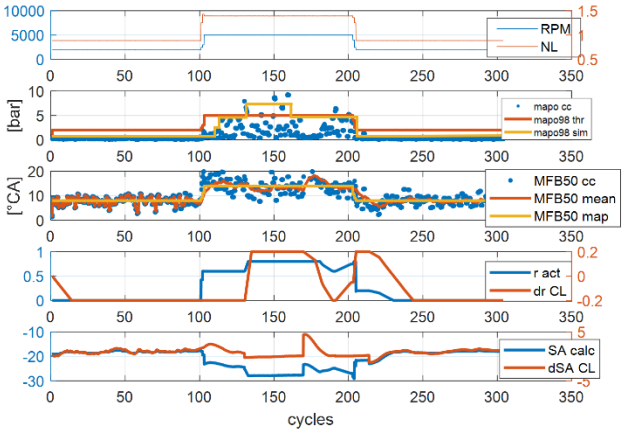

Figure 26. Transient simulation results with the CL on MFB50. Five subplots show (from top to bottom): RPM-NL, cycle-to-cycle recorded MAPO, MAPO98 and the MAPO98 threshold, cycle-to-cycle recorded MFB50, mean MFB50 and the corresponding target, the actuated *r* and the *r* correction calculated by CL chain, the actuated SA and the SA correction calculated by the CL chain.

Table 5. Root Mean Squared Errors for the validation simulations with the second version of the WI based Combustion Control.

Engine Point	RMSE MFB50 [°CA]	RMSE MAPO98 [bar]
RPM 1500 NL 0.957	0.17	0.87
RPM 2500 NL 1.43	0.32	1.89
RPM 3500 NL 1.62	0.62	1.04
RPM 4500 NL 1.3	0.45	0.93
RPM 2000-4500-2000 NL 0.88-1.49-0.88	0.88	2.34
Mean	0.49	1.41

Conclusions and Future Work

In this work an innovative WI combustion controller has been described. The proposed controller has been designed from the ground up and it is characterized by a model-based open loop part and a closed loop branch, which manages the injected water mass and the SA to control the knock level and the combustion phasing.

In the first part of the paper a new combustion model, which defines the parabolic relationship between the MFB50 and the SA, is described. Such model considers also the dependency of the mentioned relationship from the injected water mass changes. Such model is then implemented in the controller and it composes its OL branch and this is the main innovative contribution of such work. Three possible methods to implement such model in a 0-D environment are presented and compared. The polynomial approach is then chosen, thanks to its greater accuracy.

The control strategy is then thoroughly described. In particular, the algorithm utilized to define the MFB50 and *r* maps of the OL controller and the two CL systems have been presented. The CL branch is a PI-based strategy with a gain scheduling and a dynamic saturation on the TPC. The first version of the controller has a CL part that controls only the MAPO98 through the corrections on parameters *r* and SA. The second version is characterized by a CL controller with an additional branch that introduces r and SA corrections to achieve a certain MFB50 target. The MFB50TPC has been introduced to efficiently manage the two contributions that define the final SA correction. In this way, the errors committed by the combustion model can be corrected by the PI controller.

In the last part of this work the Water Injection based Combustion Control is coupled with a previously calibrated 1-D predictive combustion model and validated via SiL. The mean-cylinder combustion model has been converted in a Fast Running Model and implemented in a 0-D co-simulation environment. The two versions of the controller have been tested in RT, both under steady-state and transient conditions. The controller performance has been then evaluated with the RMSE for both controller versions, for each simulated engine point. The errors committed on the MFB50 target with the first controller are also a validation of the reliability of the proposed Combustion Model. Final results demonstrate the robustness and the accuracy of the Water Injection based Combustion Control.

The described WICC will be further developed with the introduction of an adaptive combustion model, and the experimental setup will be updated with the installation of a Rapid Control Prototyping (RCP) system, to validate the developed control system on-line at the test bench. Finally, engine block accelerometers data will be analyzed and considered as a possible solution to replace in-cylinder pressure signals, for on-board knock intensity and combustion phase measurement.

References

1. Hoppe F., Thewes M., Baumgarten H., Dohmen J., "Water injection for gasoline engines: Potentials, challenges, and solutions." International Journal of Engine Research 17, no. 1 (2016): 86-96. doi:10.1177/1468087415599867.
2. Berni, F., Breda, S., D'Adamo, A., Fontanesi, S. et al., "Numerical Investigation on the Effects of Water/Methanol Injection as Knock Suppressor to Increase the Fuel Efficiency of a Highly Downsized GDI Engine," SAE Technical Paper 2015,24-2499, 2015, doi:10.4271/2015-24-2499.
3. Battistoni, M., Grimaldi, C., Cruccolini, V., Discepoli, G. et al., "Assessment of Port Water Injection Strategies to Control Knock in a GDI Engine through Multi-Cycle CFD Simulations," SAE Technical Paper 2017-24-0034, 2017, doi:10.4271/2017-24-0034. Definitions/Abbreviations
4. Cavina, N., Rojo, N., Businaro, A., Brusa, A. et al., "Investigation of Water Injection Effects on Combustion Characteristics of a GDI TC Engine," *SAE Int. J. Engines* 10(4):2017, doi:10.4271/2017-24-0052.
5. D'Adamo, A., Berni, F., Breda, S., Lugli, M. et al., "A Numerical Investigation on the Potentials of Water Injection as a Fuel Efficiency Enhancer in Highly Downsized GDI Engines," SAE Technical Paper 2015-01-0393, 2015, doi:10.4271/2015-01-0393.
6. Rohit, A., Satpathy, S., Choi, J., Hoard, J. et al., "Literature Survey of Water Injection Benefits on Boosted Spark Ignited Engines," SAE Technical Paper 2017-01-0658, 2017, doi:10.4271/2017-01-0658.
7. Iacobacci, A., Marchitto, L., and Valentino, G., "Water Injection to Enhance Performance and Emissions of a Turbocharged Gasoline Engine under High Load Condition," SAE Int. J. Engines 10(3):2017, doi:10.4271/2017-01-0660.

8. Rahimi Boldaji, M., Sofianopoulos, A., Mamalis, S., and Lawler, B., “Effects of Mass, Pressure, and Timing of Injection on the Efficiency and Emissions Characteristics of TSCI Combustion with Direct Water Injection,” SAE Technical Paper 2018-01-0178, 2018, doi:10.4271/2018-01-0178.
9. Netzer, C., Franken, T., Seidel, L., Lehtiniemi, H. et al., “Numerical Analysis of the Impact of Water Injection on Combustion and Thermodynamics in a Gasoline Engine using Detailed Chemistry,” SAE Technical Paper 2018-01-0200, 2018, doi:10.4271/2018-01-0200.
10. Pauer, T., Martin Frohnmaier, M., Walther,J., Schenk,P., Hettinger, A.,Kampmann, R., "Optimization of Gasoline Engines by Water Injection", Internationales Wiener Motorensymposium 2016.
11. Xiao, B., Wang, S., Prucka, R.G., “A Semi-Physical Artificial Neural Network for Feed Forward Ignition Timing Control of Multi-Fuel SI Engines”, SAE Technical Paper 2013-01-0324, 2013, doi:10.4271/2013-01-0324
12. Hillion, M., Chauvin, J., Petit, N., “Open-Loop Combustion Timing Control of a Spark-Ignited Engine,” Proceedings of the 47th IEEE Conference on Decision and Control, pp 5635-5642, 2008.
13. Wang, S., Prucka, M., Dourra, H., “Model-Based Optimal Combustion Phasing Control Strategy for Spark Ignition Engines”, SAE Technical Paper 2016-01-0818, 2016, doi:10.4271/2016-01-0818
14. Businaro, A., Cavina, N., Corti, E., Mancini, G., Moro, D., Ponti, F., Ravaglioli, V., “Accelerometer Based Methodology for Combustion Parameters Estimation”, Energy Procedia, Volume 81, December 2015, Pages 950-959, https://doi.org/10.1016/j.egypro.2015.12.152
15. Gamma Technology Inc., GT Gamma Technology, 2017.
16. Cavina, N., Brusa, A., Rojo, N., and Corti, E., “Statistical Analysis of Knock Intensity Probability Distribution and Development of 0-D Predictive Knock Model for a SI TC Engine,” SAE Technical Paper 2018-01-0858, 2018, doi:10.4271/2018-01-0858.

Abbreviations

CC	Cycle-to-Cycle
CCV	Cycle to-Cycle Variability
CL	Closed Loop
FRM	Fast Running Model.
KLSA	Knock Limited Spark Advance
MAPO	Maximum Amplitude of Pressure Oscillations
MAPO98	98th MAPO percentile
MAPO98 th	98th MAPO percentile threshold
MBT	Maximum Brake Torque
MFB50	Angle corresponding to 50% of Mass Fraction Burned
MFB50TPC	Total Percentage Correction that derives from MFB50 error
nKLSA	near Knock Limited Spark Advance
NL	Net Load
OL	Open Loop
PI	Proportional Integral Controller
RMSE	Root Mean Squared Error
RT	Real Time
SA	Spark Advance
SiL	Software in the Loop
TPA	Three Pressure Analysis
TPC	Total Percentage Correction
WI	Water Injection
WICC	Water Injection based Combustion Control
WICM	Water Injection based Combustion Model